TITLE:

Redox regulation of autophagy in Arabidopsis: differential effects of reactive oxygen species.

RUNNING TITLE:

Redox regulation of autophagy

AUTHORS:

Germán Robert [1,2,3 † *], Alejandro Enet [1†], Laura Saavedra [1], Ramiro Lascano [1,2 *]

[†] Both authors contributed equally

*** Corresponding authors:**

ramiro.lascano@unc.edu.ar; robert.german@inta.gob.ar

AFFILIATIONS

[1] Plant Stress Biology Group, Unidad de Doble Dependencia INTA-CONICET (UDEA), Av. 11 de Septiembre, Córdoba 4755-X5020ICA, Argentina.

[2] Cátedra de Fisiología Vegetal, Facultad de Ciencias Exactas Físicas y Naturales, Universidad Nacional de Córdoba, Av. Velez Sarsfield 299, Córdoba, Argentina;

[3] Instituto Nacional de Tecnología Agropecuaria (INTA), Instituto de Fisiología y Recursos Genéticos Vegetales (IFRGV), Av. 11 de Septiembre, Córdoba 4755-X5020ICA, Argentina.

Alejandro Enet: ale.403@hotmail.com

Germán Robert: robert.german@inta.gob.ar

Laura Saavedra: saavedra.laura@inta.gob.ar

Ramiro Lascano: ramiro.lascano@unc.edu.ar

KEYWORDS

Autophagy, stress, reactive oxygen species, singlet oxygen, superoxide radical, hydrogen peroxide, redox state, Arabidopsis thaliana.

HIGHLIGHTS

•This research shows the differential effects of reactive oxygen species on autophagic modulation, highlighting their impact on the cytoplasmic redox state. The relationship between ROS and autophagy regulation remains unclear, and in some aspect's contradictory. Here, we present a comprehensive investigation characterizing the effects of different ROS, such as hydrogen peroxide and singlet oxygen, on the modulation of autophagy in Arabidopsis. In brief, our findings reveal differential impacts on cytoplasmic redox states and autophagic flux, providing insight into the dynamic nature of autophagy, especially in stress and post-stress conditions.

•To the best of our knowledge, our work is the first to evaluate autophagic flux both during and after oxidative stress in plants. Our results indicate that this differentiation is crucial when analyzing the effects of oxidative stress on autophagy.

ABSTRACT

Autophagy plays a key role in the responses to different stress condition in plants. Reactive oxygen species (ROS) are common modulators of stress responses, having both toxic and signaling functions. In this context, the relationship between ROS and autophagy regulation remains unclear, and in some aspects, contradictory. In this study, we employed pharmacological and genetic approaches to investigate the effects of different ROS on the cytoplastic redox state and autophagic flux in *Arabidopsis thaliana*. Ours results demonstrated that oxidative treatments with H_2O_2 and MV, which drastically increased the oxidized state of the cytoplasm, reduced the autophagic flux. Conversely, singlet oxygen, which did not have significant effects on the cytoplasmic redox state, increased the autophagic flux. Additionally, our findings indicated that after H_2O_2 and high light treatments and during the recovery period, the cytoplasm returned to its reduced state, while autophagy was markedly induced. In summary, our study unveils the differential effects of ROS on the autophagic flux, establishing a correlation with the redox state of the cytoplasm. Moreover, it emphasizes the dynamic nature of autophagy in response to oxidative stress and the subsequent recovery period.

KEYWORDS

Autophagy, stress, reactive oxygen species, singlet oxygen, superoxide radical, hydrogen peroxide, redox state, Arabidopsis thaliana.

ABBREVIATIONS

ATG: autophagy genes
Conc A: Concanamicina A
GFP: green fluorescent protein
GSH: reduced glutathione
GSSG: oxidized glutathione
MV: methyl viologen
roGFP: redox-sensitive green fluorescent proteins
ROS: reactive oxygen species

97 **INTRODUCTION**

98 Plants as sessile organisms are constantly exposed to diverse stress conditions,
99 triggering mechanisms that integrate defense and acclimation responses (Fichman and Mittler,
100 2020; Peláez-vico *et al.*, 2022). A common effect of stress is the increased production of reactive
101 oxygen species (ROS), such as superoxide (O_2^-), hydrogen peroxide (H_2O_2), singlet oxygen ($^1O_2$),
102 and the hydroxyl radical (-OH), at different subcellular compartments, such as chloroplasts,
103 mitochondria, peroxisomes, cytosol and the apoplast (Apel and Hirt, 2004; Foyer and Noctor,
104 2009, 2011*a*). Depending on their site, intensity, and duration of production, ROS can modify
105 biomolecules, influence redox signaling, and drive processes like growth, senescence, and cell
106 death. Their levels are tightly regulated by antioxidant systems, as uncontrolled ROS can lead to
107 oxidative stress (Apel and Hirt, 2004; Foyer and Noctor, 2009, 2011*b*; Trippi *et al.*, 2009).
108 Consequently, ROS are recognized as critical signaling molecules, and the cellular redox state is
109 considered an intensive property of the living system that integrates information from
110 metabolic, energetic and environmental cues controlling growth, development and acclimation
111 responses, as well as cell suicide events (Breusegem and Dat, 2006; Robert *et al.*, 2009, 2018;
112 Trippi *et al.*, 2009; Fernandez-göbel *et al.*, 2019; Fichman and Mittler, 2020; Peláez-vico *et al.*,
113 2022). In plants, chloroplast, mitochondria and peroxisome, which are redox active organelles
114 where carbon and energetic metabolisms take place, are major sources of ROS production (Apel
115 and Hirt, 2004). In chloroplasts, the photosynthetic process involves physical, biophysical, and
116 biochemical redox reactions with different reaction rates. In consequence, oxygen became a
117 potent univalent electron or energy acceptor from highly activated intermediates under
118 conditions of excess excitation energy (EEE) induced by the different stress conditions (Karpinski
119 *et al.*, 1999; Foyer and Hanke, 2022). ROS produced in the chloroplasts are particularly important
120 in the retrograde signaling of EEE conditions, affecting nuclear gene expression, acclimation
121 responses as well as programmed cell death (Karpinski *et al.*, 1999; Breusegem *et al.*, 2001;
122 Breusegem and Dat, 2006; Bechtold *et al.*, 2008; Fichman and Mittler, 2020; Foyer and Hanke,
123 2022).

124 Likewise, several stress conditions in plants have been also shown to trigger or increase
125 autophagy (Signorelli *et al.*, 2019; Wang *et al.*, 2021). Autophagy is an ancient and conserved
126 process in eukaryotes by which different cellular components are delivered to vacuole/lysosome
127 to be degraded, and is essential for plant energetic metabolism, growth, development and
128 responses to different stress conditions (Su *et al.*, 2020; Wang *et al.*, 2021). Different types of
129 autophagy have been identified in plants (Yagyu and Yoshimoto, 2023), being macroautophagy
130 (hereafter termed autophagy) the most thoroughly studied. The autophagic process is initiated,
131 and mainly modulated in the cytosol, by the formation of a double membrane cup, the
132 phagophore, that expands to engulf macromolecules and cellular components to finally form a
133 double-membrane vesicle called autophagosome. Autophagosomes are then transported and
134 fused with the vacuole, facilitating the delivery of their cargo for subsequent degradation (Yagyu
135 and Yoshimoto, 2023). The sequential steps of the autophagic process are coordinated by ATG
136 (AuTophaGy) proteins as well as by some components of the endosome pathway, as recently
137 reported (Zhuang *et al.*, 2015; Robert *et al.*, 2021). While early evidence pointed to a strong
138 transcriptionally regulation of autophagy in response to nutritional starvation conditions and
139 foliar senescence (Yoshimoto *et al.*, 2004; Breeze *et al.*, 2011), recent studies have shed light on
140 the widespread modulation of autophagy initiation and progression by post-translational
141 modifications of core autophagy proteins. These modifications primarily occur at the

142 cytoplasmic level in response to environmental cues (Feng *et al.*, 2015; Yang *et al.*, 2019; Qi *et*
143 *al.*, 2021; Agbemafle *et al.*, 2023).
144 It has been indicated a positive correlation between ROS generation and the autophagic
145 process, where ROS can serve as both sources of damage and signals (Xiong *et al.*, 2007*a*,*b*;
146 Signorelli *et al.*, 2019). Autophagy promotes the degradation of ROS-overproducing damaged
147 organelles including chloroplasts, mitochondria, and peroxisomes, thus fulfilling antioxidant
148 roles (Xiong *et al.*, 2007*b*; Shibata *et al.*, 2013; Nakamura *et al.*, 2018; Oikawa *et al.*, 2022).
149 Supporting this notion, observations in different autophagy-mutant plants demonstrate the
150 accumulation of oxidized and ubiquitinated proteins (Xiong *et al.*, 2007*a*; Munch *et al.*, 2014),
151 high levels of H_2O_2 (Yoshimoto *et al.*, 2009), increased amounts of total glutathione (Masclaux-
152 Daubresse *et al.*, 2014), accelerated senescence (Doelling *et al.*, 2002; Hanaoka *et al.*, 2002;
153 Yoshimoto *et al.*, 2004), and hypersensitivity to different stress conditions including oxidative
154 stresses (Xiong *et al.*, 2007*b*; Liu *et al.*, 2009; Zhou *et al.*, 2013), indicating a significant redox
155 imbalance. On the other hand, oxidative treatments with H_2O_2 and methyl viologen (MV) have
156 been shown to induce autophagy (Xiong *et al.*, 2007*b*; Pérez-Pérez *et al.*, 2012*b*). More recently,
157 it has been hypothesized that H_2O_2 accumulation and membrane damage may mediate
158 chlorophagy induced after UV-B and high light treatments in Arabidopsis leaves (Izumi *et al.*,
159 2017; Woodson, 2019). Consequently, it is plausible that autophagy induction occurs as a
160 response to the accumulation of cellular components that have been damaged. Notably, recent
161 studies conducted in yeast, animals and Chlamydomonas have revealed that certain proteins
162 involved in the autophagic process can be inhibited by ROS in *in vitro* experiments or artificial
163 oxidative stress *in vivo*, indicating that ROS might suppress the activity of some autophagy-
164 related proteins (Pérez-Pérez *et al.*, 2014, 2016; Frudd *et al.*, 2018; Mallén-ponce and Pérez-
165 pérez, 2023). These findings raise apparently opposite evidence regarding the autophagy
166 regulation by ROS. In this sense, a key aspect to be considered is the differential effects of ROS
167 on autophagy, which varies both during oxidative stress and after the imposition of oxidative
168 stress. Hence, the picture about the relationship among different ROS, subcellular redox
169 changes, and autophagy regulation in plants is still unclear. Under this scenario, our study aimed
170 to address the effects of different ROS on autophagy in plants, focusing on both the stress period
171 and the post-stress recovery phase.
172 Herein, we investigated the effects of different ROS on autophagy in Arabidopsis
173 seedlings. We demonstrate that oxidative treatments with H_2O_2 and MV, which drastically
174 increase cytoplasmic oxidation, suppress autophagic flux, while restoration to a reduced
175 cytoplasmic state -such as after stress subsides- correlates with the activation of autophagy. In
176 contrast, chloroplast-generated $^1O_2$ enhances autophagy without inducing statistically
177 significant changes in cytoplasmic redox state. These findings provide novel insights into the
178 complex interplay between ROS and autophagy, emphasizing the distinct roles of specific ROS
179 in regulating this critical stress response. In summary, our findings unveil the distinct effects of
180 ROS on autophagic flux, highlighting a strong correlation between autophagy and the
181 physicochemical properties of the cytoplasm. Autophagy is inhibited under highly oxidized
182 cytoplasmic conditions but is induced during recovery, likely playing a crucial role in removing
183 damaged components.
184
185
186

187 **MATERIALS AND METODS**

188 **Plant materials and growth conditions.**

189 *Arabidopsis thaliana* ecotype Columbia (Col-0) was used in this study. 35S:GFP-ATG8a transgenic
190 seeds (CS39996) (Thompson et al., 2005) were obtained from the Arabidopsis Biological
191 Resource Center. The cytosol-targeted fluorescent redox sensors GFP2-Orp1 or GRX-roGFP2
192 were provided by Dr. Markus Schwarzländer. Fluorescent (*flu*) and ferrochelatase 2 (*fc2*)
193 mutants were provided by Dr. Jesse Woodson. We introgressed the GFP-ATG8a, GFP2-Orp1 and
194 GRX-roGFP2 transgenes into the *flu* and *fc2* mutant lines by genetic crosses. Homozygous
195 offspring were then selected from the F3 backcross generations.

196 Seeds were surface-sterilized and sown on culture plates containing nutrient-rich Murashige and
197 Skoog (MS) solid medium lacking sucrose and containing 1 % agar. After sowing, plates were
198 kept in darkness at 4°C for 2 to 3 days, and then transferred to a growth chamber under a 16 h
199 light/8 h dark photoperiod. Photosynthetic photon flux density was 110 µmol m^{-2} sec^{-1}. Average
200 temperature was 22°C. Plants were grown for 7 days under these conditions and then passed to
201 MS liquid medium to carry out the different treatments. For salt and osmotic stresses, NaCl (50
202 mM) and mannitol (100 mM) were used, respectively. Oxidative treatments were performed by
203 the supplementation of the MS liquid medium with 1 µM methyl viologen (MV), 10 mM H_2O_2,
204 20 µM 3-(3,4-dichlorophenyl)-1,1-dimethylurea (DCMU), 20 µM methylene blue (MB). To
205 scavenge superoxide and peroxide, 10 mM tiron and 10 mM benzoic acid (BA) were co-
206 administrated. 10 mM dithiothreitol (DTT) was used as a reducing agent for protein disulfide
207 bonds.

208

209 **Confocal fluorescence microscopy and image analysis.**

210 Confocal microscopy was performed on an Inverted microscope Nikon Eclipse CZ1. 35S:GFP-
211 ATG8a expressing plants were observed with a 488-nm argon laser (BP 495–530 nm). To analyze
212 autophagic bodies accumulation, 1 µM Concanamycin A was added to the different treatments.
213 The number of autophagic bodies in epidermal cells was quantified after 16 h of treatments
214 using ImageJ by counting their numbers in the central vacuole of multiple cells in sections of
215 50000 μm^2. A macro for automating autophagic bodies counting was developed in ImageJ.
216 Briefly, the input images were converted into an 8-bit format, followed by background
217 subtraction using a rolling ball algorithm with a 50-pixel radius. Subsequently, particle analysis
218 was performed on the binary image, considering particle size, circularity, and displaying the
219 resulting masks.

220 Cytosol-targeted fluorescent redox sensors GFP2-Orp1 or GRX-roGFP2 were excited at 488 nm
221 and 405 nm and fluorescent emissions were collected at 505-535 nm. These transgenic plants
222 express a modified GFP sensitive to redox state (roGFP) genetically fused with different redox-
223 active proteins, the peroxidase Orp1 and Glutaredoxin GRX1, which facilitate the sensing of H_2O_2
224 and the GSH ratio, respectively (Schwarzländer *et al.*, 2009, 2015; Nietzel *et al.*, 2019). The
225 relative intensity of the two fluorescence excitation maxima depends on the redox state of
226 roGFP, allowing ratiometric measurements (ratio 405/488) independent of probe concentration
227 (Schwarzländer *et al.*, 2015; Nietzel *et al.*, 2019). roGFP predominantly equilibrates with the
228 GSSG/2GSH couple, dependent on glutaredoxins (GRX). The transcriptional fusion of roGFP with
229 GRX1 (GRX1-roGFP2) allows comparisons between different cell types and subcellular locations,
230 as it is independent of endogenous GRX availability and insensitive to a wide pH range (pH 5.5-
231 8.5) (Schwarzländer *et al.*, 2015). Thiol peroxidases (Orp1) react extremely sensitively with H_2O_2,
232 forming a sulfenic acid group and subsequently a disulfide bond. The oxidation of either of these
233 groups can then be transferred, via a thiol-disulfide exchange reaction, to reductive systems
234 such as thioredoxins or GRX, or to specific target proteins. The fusion of roGFP2 with Orp1
235 ensures that oxidation is efficiently passed from Orp1 to roGFP2. Dynamic measurements can

236 be made because, once oxidized, roGFP2-Orp1 can be reduced again by redox couples (GRX
237 and/or Thioredoxins (TRX) systems) (Schwarzländer *et al.*, 2015; Nietzel *et al.*, 2019). Therefore,
238 the redox state of roGFP2-Orp1 is influenced not only by H_2O_2 but also by reducing agents (GSH
239 and TRX). While the integration of oxidizing (H_2O_2) and reducing (GSH/TRX) influences might be
240 considered a disadvantage of the roGFP2-Orp1 probe, they reflect how the redox state of
241 endogenous thiols reactive with H_2O_2 is regulated, including the reducing capacity of the system.
242 All imaging parameters were kept constant throughout all measurements. Subsequently, a
243 single ratiometric image was generated using the ImageJ software, where the value of each pixel
244 is the product of the ratio between the intensity at 405 nm with respect to that obtained at 488
245 nm according to (Schwarzlander *et al.*, 2008). Quantitative measurements were calculated as
246 the ratio of the mean intensity from each channel. The dynamic range of these reporter lines
247 was established using 10 mM DTT and a curve of increasing concentrations of H_2O_2. For
248 pseudocolor display, the ratio was coded on a spectral color scale ranging from blue (fully
249 reduced) to red (fully oxidized).
250
251 **Immunoblot analyses.**
252 For GFP-ATG8 cleavage assay, seven-day old 35S:GFP-ATG8a transgenic plants were transferred
253 to MS liquid medium to carry out the different treatments for 6 to 8 h. Then, total proteins were
254 extracted. The extracts were centrifuged at 10 000 g for 10 min, and equal amounts of proteins
255 from the supernatants were subjected to SDS-PAGE and immunoblotted with anti-GFP
256 antibodies (Roche). Comparisons of absolute integrated density values for each line (GFP-ATG8
257 and free GFP) were made. Corresponding background values were subtracted from integrated
258 density values, then integrated density values for bands corresponding to free GFP were
259 expressed as relative values of GFP-ATG8 present in the same sample, and relativized to a
260 control condition.
261
262 **Physiological parameters.**
263 Seven-day old Arabidopsis seedlings were exposed to the different treatments for 8 h and then
264 the production of H_2O_2 and O_2^-, quantum efficiency of PSII photochemistry (ΦPSII), as well as the
265 content of chlorophyll, soluble sugars and malondialdehyde (MDA) were analyzed. To assess
266 H_2O_2 and O_2^- accumulation, leaves were stained with DAB and NBT, respectively. The staining
267 was quantified by measuring the intensity per area using ImageJ. Quantum efficiency of PSII
268 photochemistry (ΦPSII) was measured from the upper surface using a pulse amplitude
269 modulated fluorometer (FMS2, Hansatech Instruments, Pentney King's Lynn, UK).
270 Measurements were performed 6 h after the growth chamber lights were turned on. For
271 chlorophyll, soluble sugars, and MDA analysis an alcoholic extract (1:2 w/v) was obtained from
272 the samples. After centrifugation for 15 minutes at 12,000 *g*, the supernatant was diluted in
273 ethanol, and the absorbance was measured at 654 nm using a spectrophotometer. Total
274 chlorophylls were calculated following the method reported by (Wintermans M. and De Mots
275 A., 1965). For soluble sugars determination, an aliquot of the sample was dried, and
276 resuspended in a same volume of water. Then, the concentration of sugars was measured with
277 anthrone (Fales, 1951) evaluating the absorbance at 620 nm using a glucose standard curve. For
278 MDA determination, a volume of the supernatant was mixed with a same volume of a mixture
279 of 0,5 % TBA and 20 % TCA, and incubated 20 minutes at 90 °C. The mixture was centrifuged at
280 12,000 *g* for 5 minutes, and the absorbance was measured at 532 and 600 nm (Heath and Packer,
281 1968).
282
283 **RNA extraction and RT-qPCR**

284 Samples were homogenized in a cold mortar with TRIzol Reagent, mixed for 1 min and incubated
285 at room temperature for 5 min. Then, 0.2 ml chloroform per ml of TRIzol Reagent was added and
286 incubated at room temperature for 3 min. After incubation, the samples were centrifuged at 12
287 000 *g* at 4 °C for 15 min and the aqueous phases were transferred to clean tubes. RNA was
288 precipitated by adding 1 vol of isopropanol, incubated at room temperature for 10 min and
289 centrifuged at 12 000 *g* at 4 °C for 15 min. The precipitate was washed with 70 % ethanol and
290 the samples were centrifuged again at 12 000 *g* at 4 °C for 15 min. The precipitates were dried
291 and resuspended in diethyl pyrocarbonate-treated water and its concentration was quantified
292 using a NanoDrop 3300 spectrometer (Thermo Scientific). Purified RNA was treated with DNase
293 I (Invitrogen) to remove genomic DNA, according to the manufacturer's instructions. DNA-free
294 RNA (1 to 2.5 µg) was used with oligo(dT) for first strand cDNA synthesis using the Moloney
295 murine leukemia virus reverse transcriptase (M-MLV RT, Promega) according to the
296 manufacturer's instructions. For each primer pair, the presence of a unique product of the
297 expected size was checked on ethidium bromide-stained agarose gels after PCR reactions.
298 Absence of contaminant genomic DNA was confirmed in reactions with DNase-treated RNA as
299 template. The qPCR reaction was performed using iQ Universal SYBR Green Supermix (Bio-Rad).
300 Amplification of actin with the forward primer 5'-TTCAGATGCCCAGAAGTCTTG-3' and the
301 reverse primer 5-GCGATACCTGAGAACATAGTGG-3 was used to normalize the amount of
302 template cDNA. The specific primers pair employed for the detection of *Atg6* was forward primer
303 5'-AAAACTGGGAGAGCGATGAG-3' and reverse primer 5'-GATAGATGAGCCCTGCGTAG-3', for
304 *Atg4a* was 5'-CCTTTGGAATCACTCGACCCATCT-3' and 5'-ATCCGCAAACCCGTAGTTGCTT-3', for
305 *Atg7* was 5'-GCGGCTTTAGGTTTTGACAG-3' and 5'-GTTGGTCTAGAGTTCGATCAGTC -3', and for
306 *Atg5* was 5'-TCCTGTTCGGTTGTATGTTCG-3' and 5'-CGCTCTGTCTCCCATAAACTC-3'. qPCR was
307 performed in thermocycler iQ5 (Bio-Rad) at 59 °C with iQ SYBR Green Supermix (Bio-Rad),
308 according to the manufacturer's instruction. Relative transcript abundance was calculated (Livak
309 and Schmittgen, 2001).
310
311 **Microarray analysis.**
312 Publicly available microarray data were utilized to compare the expression of *Atg* genes under
313 various conditions, including nitrogen deficiency (Rubin *et al.*, 2009), treatment with 10 mM
314 H_2O_2 for 24 h (Willems *et al.*, 2016), treatment with 10 µM MV for 2 h (Scarpeci *et al.*, 2008),
315 and the examination of *flu* mutant plants subjected to an 8-hour cycle of darkness followed by
316 2 h of light (Op Den Camp *et al.*, 2003). Expression values were normalized to the corresponding
317 control conditions employed in each study and were expressed as $\log_2$ values.
318
319 **Statistical analyses.**
320 Data were analysed by analysis of variance (ANOVA) followed by the Di Rienzo–Guzman–
321 Casanoves (DGC) test model, a cluster-based method for identifying groups of non-
322 homogeneous means, using InfoStat software (Di Rienzo *et al.*, 2002).
323
324
325 **RESULTS**
326 **H_2O_2 and methyl viologen treatments induced cytoplasmic oxidation and inhibited**
327 **autophagy in Arabidopsis.**
328 Initially, to gain insights into the interplay between ROS, redox state changes and
329 autophagy, *Arabidopsis thaliana* seedlings were subjected to well-established autophagy-
330 inducing conditions, namely nutritional starvation and different abiotic stress treatments (Wang
331 *et al.*, 2021), and both autophagy and the cytoplasmic redox state were analyzed (Fig. 1). To
332 monitor autophagy, 35S:GFP-ATG8a (GFP-ATG8) transgenic plants were grown 7 days in MS solid

333 medium, and then transferred to the different treatments in MS liquid medium supplemented
334 with 1 µM Concanamycin A (Conc A) for a 16 hour-period. Conc A is a V-ATPase inhibitor widely
335 used to prevent vacuole acidification, thereby effectively inhibiting the lytic activity of vacuoles,
336 thus allowing the detection of autophagic bodies accumulation into the vacuoles through
337 confocal microscopy (Fig. 1A and B). Analysis of autophagic flux using Conc A better defines
338 autophagic activity since the increase of autophagosome number in the cytoplasm does not
339 necessarily corresponds to an enhanced autophagic activity (Robert *et al.*, 2021). When
340 subjected to carbon and nitrogen starvation treatments, epidermal cells showed a high
341 accumulation of autophagic bodies in the vacuole compared to control conditions, indicating an
342 activated autophagic flux (Fig. 1A and B). Similarly, saline and osmotic stress treatments resulted
343 in comparable outcomes, with a significant increase in autophagic bodies accumulating within
344 the vacuoles (Fig. 1A and B). Besides, to evaluate the cytoplasmic redox state *in vivo*, 7 days old
345 transgenic plants expressing the cytosol-targeted fluorescent redox sensors GFP2-Orp1 or GRX-
346 roGFP2 were subjected to the different treatments (Fig. 1). These transgenic plants express a
347 redox-sensitive green fluorescent protein (roGFPs) genetically fused to different redox-active
348 proteins, responsive to H_2O_2 production and GSH:GSSG, respectively (Schwarzländer *et al.*, 2009;
349 Aller *et al.*, 2013; Schwarzla *et al.*, 2015; Nietzel *et al.*, 2019). The relative intensity of the two
350 fluorescence excitation maxima depends on the redox state of the modified GFP, enabling
351 ratiometric measurements, independent of the probe concentration (Schwarzländer *et al.*,
352 2015) (more details in *Materials and Methods*). The dynamic range of these reporter lines was
353 previously monitored using DTT and H_2O_2 (Fig. S1A). Notably, in epidermal cells of seedlings
354 expressing either GFP2-Orp1 or GRX-roGFP2, no changes in the cytoplasmic redox state were
355 detected after 16 h of nutritional starvation, neither under saline or osmotic stress treatments
356 compared to control conditions (Fig. 1A and C). These findings align with earlier and recent
357 assessments of the redox state in cells of GRX-roGFP2 and roGFP2-ORP1 transgenic plants under
358 water deficit and saline stress conditions (Schwarzländer *et al.*, 2009; Bohle *et al.*, 2024).
359 To further investigate the interplay between ROS, redox state changes and autophagy,
360 oxidative stress treatments using H_2O_2 and methyl viologen (MV) were conducted. We evaluated
361 different concentrations of H_2O_2 and observed a dose-dependent response for both the
362 cytoplasmic redox state and autophagy inhibition. A similar approach was taken with MV, an
363 herbicide widely used for the induction of photooxidative stress as it takes electrons from
364 photosystem I, generating O_2^- and H_2O_2 inside chloroplasts in the presence of light (Mehler,
365 1951; Farrington *et al.*, 1973; Lascano *et al.*, 2012; Nazish *et al.*, 2022) (Fig. S1B-D). Based on
366 these results and with the intention of employing moderate oxidative stress conditions that do
367 not induce cell death, we used 10 mM H_2O_2 and 1 µM MV for subsequent experiments. Although
368 oxidative treatments have been reported as autophagy-inducing conditions in Arabidopsis and
369 Chlamydomonas (Xiong *et al.*, 2007*b*; Pérez-Pérez *et al.*, 2012*b*), no significant differences were
370 observed in the accumulation of autophagic bodies in the epidermal cells of seedlings treated
371 with MV or H_2O_2 for 16 h compared to the control condition (Fig. 1A and B). In contrast to
372 observations under autophagy-inducing conditions such as nutritional starvation, saline, or
373 osmotic stresses, these oxidative treatments significantly oxidized the cytoplasmic redox state,
374 as revealed by analyzing both GRX-roGFP2 and roGFP2-ORP1 plants, as well as DAB staining, a
375 histochemical reagent for H_2O_2 (Fig. 1A and C; Fig. S1; Fig. S2) (Fernandez-göbel *et al.*, 2019).
376 To further characterize the effects of oxidative stress on autophagy, treatments with MV
377 and H_2O_2 were performed on 35S:GFP-ATG8a plants under autophagic inducing conditions,
378 specifically nitrogen and carbon starvation (Fig. 2, Fig. S2). Interestingly, the addition of 1 µM
379 MV or 10 mM H_2O_2 during the 16-hour starvation treatments significantly reduced the
380 accumulation of autophagic bodies (Fig. 2A and B). Furthermore, the inhibitory effects of the

381 oxidative treatments on the autophagic flux were also confirmed by analyzing the degradation
382 of the GFP-ATG8a fusion protein by western blot. This analysis provides insight beyond the
383 cellular level, extending to the organ or plant level (Fig. 2D, Fig. S2). Furthermore, the evaluation
384 of autophagic flux through the analysis of the degradation of the GFP-ATG8 fusion protein by
385 immunoblotting allowed us to examine the effects of oxidative stress on autophagy in shorter
386 time periods (6-8 h, Fig. 2D). Next, tiron and benzoic acid were co-administered with the MV
387 treatment to scavenge superoxide and hydrogen peroxide, respectively (Navabpour *et al.*, 2003;
388 Mansouri *et al.*, 2005; Velika and Kron, 2012; Liubimovskii *et al.*, 2021). The effects of MV on
389 autophagic flux, H_2O_2 accumulation, and cytoplasmic redox state were blocked in the presence
390 of ROS scavengers (Fig. 2, Fig. S2A and B). Similarly, photooxidative stress induced by high light
391 treatments showed an inhibitory effect on the autophagy flux, which was reversed in the
392 presence of the superoxide radical scavenger, tiron (Fig. 2D). Moreover, both tiron and benzoic
393 acid prevented photosynthetic damage caused by MV treatments, as measured by the quantum
394 yield of photosystem II (ΦPSII), and prevented the decrease in soluble sugar levels (Fig. S2C).
395 Furthermore, the inhibitory effects of MV on autophagic flux and the oxidation of the GSH:GSSG
396 sensor probe (GRX-roGFP2) were reversed when 10 mM dithiothreitol (DTT), a reducing agent
397 for protein disulfide bonds, was added (Fig. S2A and B). These results emphasize that the effects
398 of MV in plants are associated with its capacity to induce ROS generation, contributing to a more
399 oxidized cellular redox state and oxidative damage (Lascano *et al.*, 2012). Notably, the
400 restoration of autophagic flux in MV-treated plants by tiron, benzoic acid, and DTT suggests that
401 H_2O_2 may inhibit autophagy, potentially by oxidizing disulfide bonds in crucial ATG proteins (Fig.
402 S3 and S4) as demonstrated in recent studies in yeast, Chlamydomonas, and animals (Pérez-
403 Pérez *et al.*, 2014, 2016; Frudd *et al.*, 2018; Zheng *et al.*, 2020; Mallén-ponce and Pérez-pérez,
404 2023). H_2O_2 treatments inhibited autophagy in plant seedlings, roots, shoots, and detached
405 mature leaves under carbon or nitrogen starvation conditions (Fig. S2D). Although the intensity
406 of this effect may vary depending on the organ and developmental stage, probably due to
407 differences in baseline redox states and cellular contexts for stress responses, these
408 observations suggest a robust inhibitory role of H_2O_2 across various plant tissues.
409
410 **Autophagy is induced in the recovery phase after oxidative stress in Arabidopsis.**
411 Previous reports indicated that autophagy is involved in degrading oxidized proteins and
412 organelles in response to oxidative stress (Xiong *et al.*, 2007*b*; Shibata *et al.*, 2013; Izumi *et al.*,
413 2017; Oikawa *et al.*, 2022). However, our experimental results demonstrate that oxidative stress
414 treatments inhibit autophagy. Considering these findings, we aimed to investigate autophagic
415 activity following oxidative stress treatments by assessing the autophagic flux in Arabidopsis
416 plants during the recovery phase. With this purpose, 7-day-old Arabidopsis seedlings were
417 subjected to a brief exposure of 10 mM H_2O_2 or high light intensity (≈1000 µmoles m^{-2} s^{-1}) for 4
418 hours, followed by transfer to H_2O_2-free MS liquid medium under control conditions (≈100
419 µmoles m^{-2} s^{-1}) for a 20-hour recovery period. Additionally, a set of plants were incubated in 10
420 mM H_2O_2 or to control conditions (H_2O_2-free MS liquid medium) for 24 h. This experimental
421 design aimed to elucidate the dynamic changes in autophagy following oxidative stress and
422 determine whether autophagic activity is modulated during the recovery phase. The results
423 showed that autophagic flux was inhibited in plants incubated 24 h with H_2O_2 compared to
424 control conditions (Fig. 3A, B and D). Interestingly, autophagic flux was not only recovered but
425 also induced during the recovery period after the oxidative stress treatments surpassing the
426 levels observed in plants subjected to control conditions (Fig. 3A, B and D). Likewise, after the
427 20-hour recovery period, the redox biosensors returned to their reduced state, indicating

428 cytoplasmic redox recovery, and a well-defined correlation between the reduced cytoplasmic
429 redox state and autophagic flux (Fig. 3A and C).

430 **Singlet oxygen induced autophagic flux without effect on the cytoplasmic redox state.**

431 Singlet oxygen ($^1O_2$) is mainly produced in the chloroplast, and its targets are
432 predominantly confined inside this organelle due to the specific physicochemical characteristic
433 of this ROS (Dmitrieva *et al.*, 2020). To investigate the effects of $^1O_2$ on the autophagic activity,
434 GFP-ATG8a seedlings were treated with 3-(3,4-dichlorophenyl)-1,1-dimethylurea (DCMU) (Fig.
435 4), an herbicide that specifically induces $^1O_2$ generation by blocking the electron transport chain
436 in photosystem II and inhibiting the plastoquinone reduction. It has been reported that DCMU
437 promotes $^1O_2$ generation without affecting superoxide anion and hydroxyl radicals at PSII
438 (Fufezan *et al.*, 2002; Flors *et al.*, 2006; Dmitrieva *et al.*, 2020). The analysis of autophagic body
439 accumulation and cytoplasmic redox state was conducted after a 16-hour treatment (Fig. 4A-C).
440 Additionally, treatments with methylene blue (MB), a type-II photosensitizer able to generate
441 $^1O_2$ in leaves under visible light (Shao *et al.*, 2007, 2013), with minor effects on photosynthesis
442 (Fig. 4E), were also performed. Treatments with these chemicals increased the accumulation of
443 autophagic bodies but did not show statistically significant effects on the redox state of the
444 cytoplasm in Arabidopsis cells compared to control treatment (Fig. 4A and B). The autophagic
445 flux-inducing effect of DCMU and MB was also evidenced after 6-8 hours of treatments through
446 the analysis of GFP-ATG8 degradation by immunoblotting (Fig. 4D).

447 To further investigate the effects of $^1O_2$ on the autophagic process, we performed
448 experiments with widely used endogenously chloroplast $^1O_2$-hyperproducing *Arabidopsis*
449 mutant plants: fluorescent (*flu*) and two different lines of ferrochelatase 2 (*fc2*), *fc2.1* which
450 presents reduced expression levels of *Fc2*, and the null mutant *fc2.2*. These mutant plants
451 accumulate different photosensitizing intermediates of chlorophyll biosynthesis in the dark,
452 which, upon light exposure lead to an exacerbated production of $^1O_2$ (Op Den Camp *et al.*, 2003).
453 The *flu* mutant plants accumulate protochlorophyllide (Meskauskiene *et al.*, 2001), while
454 mutations in plastid ferrochelatase 2 lead to the accumulation of protoporphyrin IX
455 (Scharfenberg *et al.*, 2015). Likewise, these genotypes were crossed with autophagy reporter-
456 and redox sensor-transgenic plants. Initially, wild type, *flu* and *fc2* mutant plants were grown 7
457 days under continuous light conditions (control conditions), and several growth and
458 physiological parameters were evaluated (Fig. S6). Interestingly, the *fc2* mutants showed
459 arrested root growth, reduced chlorophyll levels, increased levels of malondialdehyde (MDA),
460 an intermediary metabolite of lipid peroxidation used as oxidative stress marker (Robert *et al.*,
461 2014), and reduced levels of soluble sugars compared to wild type, while no significant
462 differences were observed between wild type and *flu* mutant (Fig. S6). Likewise, the cytoplasmic
463 redox state in *fc2* plants was significantly more oxidized than that in the wild type and *flu*
464 backgrounds (Fig. S6, Fig. 5). Furthermore, and consistent with a previous study (Lemke *et al.*,
465 2021), the autophagic flux was induced in *fc2* mutants plants compared to wild type and *flu*
466 mutant under continuous light (control) conditions (Fig. S6). Hence, considering the altered
467 phenotypes observed in *fc2* mutants even under control conditions, we used the *flu* mutants for
468 subsequent analysis.

469 *flu*/GFP-ATG8a plants were grown under continuous light conditions for 7 days,
470 transferred to darkness for 8 h, and then re-exposed to light in the presence of Conc A for
471 another 6-8 h. After the light/dark/light cycling conditions, a significantly increased autophagic
472 flux was observed in *flu*/GFP-ATG8a compared to Col-0/GFP-ATG8 plants. However, no
473 statistically significant differences were observed among these genotypes under continuous
474 light conditions (Fig. 5A, B and D). Besides, the cytoplasmic redox state was monitored under
475 control conditions as well as after a period of darkness by analyzing the fluorescent redox sensor

476 roGFP2-ORP1 expressed in the wild type and *flu* backgrounds. Although a slight tendency
477 towards a more oxidized state was observed in the cytoplasm of *flu* mutant plants once re-
478 exposed to light, the differences were not statistically significant (Fig. 5C). Thus, in contrast to
479 H_2O_2 and MV treatments, $^1O_2$ increased the autophagic flux and did not oxidize the cytoplasmic
480 redox state, indicating differential effects on the autophagic activity depending on the ROS
481 nature, subcellular site of action, and their effects on the cytoplasmic redox state. Additionally,
482 the transcript levels of *Atg4*, *Atg5*, *Atg6* and *Atg7* were analyzed by RTq-PCR in *flu* mutant after
483 8 h of light re-exposure. No statistically significant differences were observed in the expression
484 level of the analyzed genes between wild type and *flu* mutant neither under control conditions
485 nor after cycling conditions (Fig. S7).
486
487 **DISCUSSION**
488 Plants, as photosynthetic, aerobic and sessile organisms, naturally produce reactive
489 oxygen species (ROS) as byproducts of various metabolic processes, especially when exposed to
490 environmental stresses. Due to their high reactivity, ROS play dual roles, acting as agents of
491 damage and as signaling molecules. Consequently, ROS are universally implicated in plant stress
492 symptomatology, and also play a pivotal role in modulating plant growth, development, and cell
493 death (Apel and Hirt, 2004; Trippi *et al.*, 2009; Baxter *et al.*, 2014; Choudhury *et al.*, 2017;
494 Fichman and Mittler, 2020). Similarly, a variety of stress conditions in plants have been
495 demonstrated to initiate or enhance autophagy (Bassham *et al.*, 2006; Liu *et al.*, 2009; Signorelli
496 *et al.*, 2019; Su *et al.*, 2020). Moreover, defects in antioxidant proteins in Arabidopsis and
497 Chlamydomonas contribute to uncontrolled ROS bursts and autophagy induction (Pérez-Pérez
498 *et al.*, 2012*a*; Shibata *et al.*, 2013). While the concurrent induction of ROS production and
499 autophagy activation suggests a positive correlation between these cellular processes, certain
500 molecular mechanisms reported in animal cells, yeast, and Chlamydomonas, indicate that ROS
501 may also negatively influence on autophagy (Pérez-Pérez *et al.*, 2014, 2016; Frudd *et al.*, 2018;
502 Mallén-ponce and Pérez-pérez, 2023). However, direct evidence of ROS-mediated inhibition of
503 autophagy in plants remains scarce. Additionally, it is important to consider whether autophagy
504 is activated directly by ROS signaling or as a response to cellular damage induced by ROS,
505 potentially creating a feedback loop between ROS production and autophagic activity.
506 Furthermore, existing literature often treats ROS as a homogeneous group, overlooking the
507 potential differences in how distinct types of ROS impact autophagy, and not consistently
508 distinguishing their effects during stress imposition versus recovery phases in plants. Our
509 findings point in that direction, highlighting the differential effects of ROS on autophagy, and
510 suggesting that under specific stress conditions leading to a highly oxidized cytoplasmic state,
511 the autophagic process may be suppressed. Additionally, the impact of ROS on autophagy is
512 likely influenced by the developmental stage and the specific organ, as these factors determine
513 both the baseline redox state and the cellular context for stress responses. Once the oxidative
514 stress subsides and the cytoplasmic redox status is restored, autophagy is activated, potentially
515 facilitating the removal of damaged cellular components.
516 The relationship between autophagy and ROS is intricate, and our findings revealed that
517 different types of ROS, even when generated in the same organelle, can have different effects
518 on the autophagic process. We observed that under conditions of nutritional starvation, which
519 are canonical inducers of autophagy, oxidative treatments with MV and H_2O_2, that led to
520 significant oxidation of the cytoplasmic redox state, had an inhibitory effect on the autophagic
521 flux (Fig. 2). This implies that the comparatively limited autophagosome biogenesis rate under
522 optimal growth conditions could potentially account for the absence of observable inhibitory
523 effects of ROS on autophagy in prior *in vivo* plant studies (Fig. 1). Opposite to the inhibitory

524 effects of H_2O_2 on the autophagic flux, the specific generation of $^1O_2$ in the *flu* mutant plants, as
525 well as treatments with DCMU and MB (Fufezan *et al.*, 2002; Op Den Camp *et al.*, 2003; Flors *et*
526 *al.*, 2006; Shao *et al.*, 2007, 2013; Dmitrieva *et al.*, 2020), increased the autophagic activity (Fig.
527 4 and Fig. 5). These findings are consistent with previous research demonstrating that
528 treatments with norflurazon, an inhibitor of carotenoid biosynthesis, triggers autophagy in
529 *Chlamydomonas reinhardtii* (Pérez-Pérez *et al.*, 2012*a*, 2016). Similarly to what is observed in *flu*
530 mutants (Op Den Camp *et al.*, 2003), norflurazon treatments lead to perturbations in plastid
531 homeostasis that increase the photosensitizing activity of tetrapyrroles, which can transfer the
532 excitation energy to the oxygen molecule, thereby generating $^1O_2$ (Kim and Apel, 2013). Singlet
533 oxygen, carotenoid derivatives, and tetrapyrroles are principal components of the retrograde
534 signaling pathway, a key process that regulates not only chloroplastic processes but also
535 intersects with other cellular signaling events playing broader roles in plant function (Chan *et*
536 *al.*, 2016).

537 The distinct effects of $^1O_2$ and H_2O_2 on autophagy are likely driven by their unique
538 chemical properties, reactivities, and molecular targets. $^1O_2$, being highly reactive and short-live,
539 primarily acts near its generation site. Consequently, no significant redox changes were
540 observed in the cytoplasm following DCMU and MB treatments or in *flu* mutants (Fig. 4 and 5).
541 This ROS primarily predominantly reacts with unsaturated fatty acids, generating
542 hydroperoxides that disrupt lipid membranes and potentially signal damage, being the major
543 ROS involved in photooxidative damage (Triantaphylidès *et al.*, 2008). Chloroplastic membrane
544 damage, in particular, may trigger specific autophagy-activating signals (Izumi *et al.*, 2017;
545 Nakamura *et al.*, 2018). Conversely, treatments with MV and H_2O_2, which reduced autophagic
546 flux, significantly oxidized the cytoplasmic redox state (Fig. 1 and Fig. 2). These findings establish
547 a clear correlation between the cytoplasmic redox status and autophagic flux. H_2O_2 is less
548 reactive but more diffusible than $^1O_2$, allowing it to oxidize thiol groups in cysteine residues of
549 proteins throughout the cell, leading to structural and functional alterations. Supporting this,
550 MV and H_2O_2 -induced oxidation of the cytoplasmic redox state, which could be reversed by ROS
551 scavengers such as tiron or benzoic acid, as well as by the disulfide bond reductant DTT. These
552 observations suggest that H_2O_2 not only inhibits autophagy but also implicates protein oxidation
553 in this response. At the molecular level, the activity of key ATG proteins has been demonstrated
554 to be subjected to redox regulation, being the proteins active when reduced and inactive when
555 oxidized. Different cysteine residues have been identified as targets for redox regulation (Figs.
556 S3 and S4). For example, the protease ATG4 which cleaves ATG8 for lipidation and delipidation
557 with PE, is inhibited by H_2O_2 in *Saccharomyces cereivisiae* and *Chlamydomonas reinhardtii*. This
558 inhibition involves Cys400 and Cys338 in Chlamydomonas and yeast, respectively (Pérez-Pérez
559 et al., 2014, 2016). Reducing agents like DTT can restore ATG4 activity (Pérez-Pérez et al., 2014,
560 2016). Similarly, oxidation of ATG3 and ATG7, leads to the formation of an intermolecular
561 disulfide-bound complex between Cys264 in ATG3 and Cys572 in ATG7, inhibiting ATG8
562 lipidation in animal cells and recently observed in Chlamydomonas (Frudd *et al.*, 2018; Mallén-
563 ponce and Pérez-pérez, 2023). The presence of these amino acid residues among ATG protein
564 isoforms in yeast, human cells, Chlamydomonas and Arabidopsis (Figs. S3 and S4) suggests that
565 similar redox regulation may also occur in plants. These conserved cysteines and others
566 identified as potential redox candidates (Figure S4) are targets to analyze in future studies.

567 The complexity of the relationship between autophagy and ROS increases when
568 considering that autophagy plays a critical role in degrading oxidized proteins and damaged
569 organelles, which, in turn, are both products of oxidative stress and primary sources of ROS
570 production. This highlights a feedback loop where the degradation of ROS-damaged organelles
571 via autophagy helps mitigate further ROS generation, yet the oxidative damage to these

572 organelles also drives the need for autophagic degradation. A crucial question in this context is
573 to what extent autophagy activation under oxidative stress is directly regulated by ROS or arises
574 as a secondary response to ROS-induced damage. ROS can directly influence autophagic process
575 through redox modifications of key proteins involved in the autophagy machinery. Paradoxically,
576 it has been shown that oxidation of ATG components from yeast, animals and Chlamydomonas
577 exerts a negative regulatory effect on their activity (Pérez-Pérez *et al.*, 2014, 2016; Frudd *et al.*,
578 2018; Mallén-ponce and Pérez-pérez, 2023). In parallel, oxidative stress causes cellular damage,
579 such as the oxidation of proteins, lipids, and nucleic acids, or the disruption of organellar
580 integrity. These byproducts of oxidative damage may act as signals that trigger autophagy as
581 part of a cellular clearance and repair mechanism (Izumi *et al.*, 2017; Nakamura *et al.*, 2018,
582 2021). Understanding the balance between these direct and indirect pathways is critical to
583 dissect the precise role of ROS in regulating autophagy. Our assessment of autophagic flux aimed
584 to dissect this relationship, shedding light on the role of autophagy in cellular adaptation to
585 oxidative stress and its recovery. Previous research has shown that photodamage-inducing
586 treatments, such as high-intensity or UV-B light irradiation, stimulate chloroplast degradation
587 *via* autophagy, while antioxidants treatments inhibited autophagy induction, suggesting that
588 ROS accumulation or the resulting damage plays a role in triggering this process (Izumi *et al.*,
589 2017). In our experiments, we observed increased autophagic flux during the recovery period
590 after oxidative stress exposure, concurrent with the restoration of a reduced redox state in the
591 cytoplasm, indicating that the autophagy inhibition caused by O_2^-/H_2O_2 is transient (Fig. 3). Our
592 findings also suggest that the induction of autophagy after oxidative stress subsides is associated
593 with the clearance of damaged cytoplasmic components, as evidenced by treatments with the
594 antioxidants tiron and benzoic acid (Fig. S2C). These treatments decreased ROS production and
595 mitigated cell injury, supporting the idea that autophagy plays a critical role in resolving
596 oxidative damage. Additionally, the transcript analysis of *ATG* genes supports the notion that
597 the observed inhibitory redox regulation primarily operates at a post-transcriptional and/or
598 post-translational level. This aligns with existing literature suggesting oxidative modifications
599 negatively impact the ATG machinery's functionality, although further studies are required to
600 confirm and explore these dynamics. Overall, these findings underscore the dynamic nature of
601 autophagy in response to oxidative stress and recovery, suggesting a complex regulatory
602 mechanism in plants.
603 In summary, our work provides a novel perspective on the relationship between ROS
604 and autophagy. The distinct effects of H_2O_2 and $^1O_2$ on autophagy underscore that the term
605 "ROS" encompasses a diverse group of molecules impacting on this process in fundamentally
606 different ways. While the relationship between ROS and autophagy in plants has been the focus
607 of numerous studies, many investigations have treated ROS as a homogeneous category. This
608 approach, while valuable in establishing foundational insights, may overlook the distinct effects
609 that specific ROS types exert on autophagic processes. Our findings align with previous studies
610 suggesting that H_2O_2 and $^1O_2$ have antagonistic effects on plant stress responses (Karpinska *et*
611 *al.*, 2000; Laloi *et al.*, 2007; Triantaphylidès *et al.*, 2008; Melchiorre *et al.*, 2009; Sabater and
612 Martín, 2013). The differential effects of these ROS on autophagic flux observed in this study are
613 consistent with earlier reports demonstrating distinct impacts of H_2O_2 and $^1O_2$ on the activity of
614 ATG4, reflected in the levels of lipidated ATG8 after treatments with H_2O_2 or norflurazon (Pérez-
615 Pérez *et al.*, 2016). These results highlight the potential for specific ROS to exert unique
616 regulatory roles in the modulation of autophagy. Recognizing these nuances provides a deeper
617 understanding of the intricate interplay between ROS signaling and autophagic processes.
618 Further research should employ more advanced methodologies, such as quantitative global
619 analysis through mass spectrometry or electron paramagnetic resonance (EPR), to precisely

measure ROS dynamics in plants subjected to abiotic stress. These approaches are essential to correlate the relative abundance of distinct ROS with autophagy modulation, ultimately shedding light on their roles in modulating autophagy in response to fluctuating environmental conditions.

SUPPLEMENTARY DATA

Supplementary Figure 1: Optimization of methyl viologen (MV) and H_2O_2 concentrations, and calibration of the redox sensors.
Supplementary Figure 2: DTT, tiron and benzoic acid reversed the effects of MV treatments.
Supplementary Figure 3: Sequence alignment of ATG4 proteases from different organisms.
Supplementary Figure 4: Sequence alignment of ATG3 and ATG7 proteins from different organisms.
Supplementary Figure 5: Characterization of *fc2* and *flu* mutant plants under continuous light conditions.
Supplementary Figure 6: Transcript level of *Atg* genes in Arabidopsis plants subjected to different oxidative treatments.

ACKNOWLEDGEMENTS

We thank Dr. Leandro Ortega, Dra. Virginia Lobatto and Dra. Anahí Yañez (Unidad de Doble Dependencia INTA-CONICET (UDEA)) for helpful support with the confocal microscopy and for technical support. We also thank Sistema Nacional de Microscopia of the Ministerio de Ciencia, tecnología e innovación Productiva (MINCyT), Argentina.

AUTHOR CONTRIBUTION:

GR and RL: conceptualization; GR and AE: investigation; GR, AE, LS and RL: formal analysis; GR, LS, and RL: resources; GR and AE: writing original draft and incorporated feedback from all authors; GR and AE: visualization; GR and RL: supervision; GR, LS and RL: funding acquisition.

CONFLICT OF INTEREST

No conflict of interest declared.

FUNDING

This work was supported by grants from Agencia Nacional de Promoción Científica y Tecnológica, Argentina: FONCYT-PICT-2019-0533 (RL), FONCyT PICT-2017-2863 (GR), and FONCyT PICT-2020-2482 (LS); Consejo Nacional de Investigaciones Científicas y Técnicas CONICET-PIP2015-PIP2019 (RL), Proyecto INTA 2019-PD-E6-I116-001 (RL and GR), Proyecto INTA 2023-PD-L03-I084 and Proyectos Consolidar, Secretaría de Ciencia y Técnica de la Universidad Nacional de Córdoba (UNC) (RL).

REFERENCES

Agbemafle W, Wong MM, Bassham DC. 2023. Transcriptional and post-translational regulation of plant autophagy. Journal of Experimental Botany **74**, 6006–6022.
Aller I, Rouhier N, Meyer AJ. 2013. Development of roGFP2-derived redox probes for measurement of the glutathione redox potential in the cytosol of severely glutathione-deficient rml1 seedlings. Frontiers in Plant Science **4**, 1–12.
Apel K, Hirt H. 2004. Reactive oxygen species: metabolism, oxidative stress, and signal transduction. Annual review of plant biology **55**, 373–99.
Bassham DC, Laporte M, Marty F, Moriyasu Y, Ohsumi Y, Olsen LJ, Yoshimoto K. 2006.

669 Autophagy in Development and Stress Responses of Plants. Autophagy **2**, 2–11.
670 **Baxter A, Mittler R, Suzuki N**. 2014. ROS as key players in plant stress signalling. Journal of
671 experimental botany **65**, 1229–1240.
672 **Bechtold U, Richard O, Zamboni A, Gapper C, Geisler M, Pogson B, Karpinski S, Mullineaux**
673 **PM**. 2008. Impact of chloroplastic- and extracellular-sourced ROS on high light-responsive gene
674 expression in Arabidopsis. Journal of experimental botany **59**, 121–33.
675 **Bohle F, Klaus A, Tegethof H, Schwarzländer M, Hochholdinger F, Meyer AJ, Acosta IF,**
676 **Müller-Schüssele SJ**. 2024. Contrasting cytosolic glutathione redox dynamics under abiotic and
677 biotic stress in barley as revealed by the biosensor Grx1-roGFP2. Journal of experimental
678 botany **75**, 2299–2312.
679 **Breeze E, Harrison E, McHattie S, *et al.*** 2011. High-resolution temporal profiling of transcripts
680 during Arabidopsis leaf senescence reveals a distinct chronology of processes and regulation.
681 Plant Cell **23**, 873–894.
682 **Breusegem F Van, Dat JF**. 2006. Reactive Oxygen Species in Plant Cell Death. Plant physiology
683 **141**, 384–390.
684 **Breusegem F Van, Vranova E, Dat JF, Inze D**. 2001. The role of active oxygen species in plant
685 signal transduction. Plant Science **161**, 405–414.
686 **Chan KX, Phua SY, Crisp P, McQuinn R, Pogson BJ**. 2016. Learning the Languages of the
687 Chloroplast: Retrograde Signaling and beyond. Annual Review of Plant Biology **67**, 25–53.
688 **Choudhury FK, Rivero RM, Blumwald E, Mittler R**. 2017. Reactive oxygen species, abiotic
689 stress and stress combination. Plant Journal **90**, 856–867.
690 **Dmitrieva VA, Tyutereva E V., Voitsekhovskaja O V.** 2020. Singlet oxygen in plants:
691 Generation, detection, and signaling roles. International Journal of Molecular Sciences **21**.
692 **Doelling JH, Walker JM, Friedman EM, Thompson AR, Vierstra RD**. 2002. The APG8/12-
693 activating enzyme APG7 is required for proper nutrient recycling and senescence in
694 Arabidopsis thaliana. Journal of Biological Chemistry **277**, 33105–33114.
695 **Fales FW**. 1951. The assimilation and degradation of carbohydrates by yeast cells. The Journal
696 of biological chemistry **193**, 113–124.
697 **Farrington JA, Ebert M, Land EJ, Fletcher K**. 1973. Bipyridylium quaternary salts and related
698 compounds. V. Pulse radiolysis studies of the reaction of paraquat radical with oxygen.
699 Implications for the mode of action of bipyridyl herbicides. Biochimica et Biophysica Acta **314**,
700 372–381.
701 **Feng Y, Yao Z, Klionsky DJ**. 2015. How to control self-digestion: transcriptional, post-
702 transcriptional, and post-translational regulation of autophagy. Trends in cell biology **25**, 354–
703 363.
704 **Fernandez-göbel TF, Deanna R, Muñoz NB, Robert G, Asurmendi S, Lascano R**. 2019. Redox
705 Systemic Signaling and Induced Tolerance Responses During Soybean – Bradyrhizobium
706 japonicum Interaction : Involvement of Nod Factor Receptor and Autoregulation of
707 Nodulation. Frontiers in Plant Science **10**, 1–15.
708 **Fichman Y, Mittler R**. 2020. Rapid systemic signaling during abiotic and biotic stresses: is the
709 ROS wave master of all trades? Plant Journal **102**, 887–896.
710 **Flors C, Fryer MJ, Waring J, Reeder B, Bechtold U, Mullineaux PM, Nonell S, Wilson MT,**
711 **Baker NR**. 2006. Imaging the production of singlet oxygen in vivo using a new fluorescent
712 sensor, Singlet Oxygen Sensor Green. Journal of experimental botany **57**, 1725–34.
713 **Foyer CH, Hanke G**. 2022. ROS production and signalling in chloroplasts: cornerstones and
714 evolving concepts. Plant Journal **111**, 642–661.
715 **Foyer CH, Noctor G**. 2009. Redox Regulation in Photosynthetic Organisms: signaling,
716 acclimation, and practical implications. Antioxidants & Redox Signaling **11**, 861–905.
717 **Foyer CH, Noctor G**. 2011*a*. Ascorbate and glutathione: the heart of the redox hub. Plant
718 physiology **155**, 2–18.
719 **Foyer CH, Noctor G**. 2011*b*. Ascorbate and glutathione: the heart of the redox hub. Plant
720 physiology **155**, 2–18.

721 **Frudd K, Burgoyne T, Burgoyne JR**. 2018. Oxidation of Atg3 and Atg7 mediates inhibition of
722 autophagy. Nature Communications **9**, 1–15.
723 **Fufezan C, Rutherford AW, Krieger-liszkay A**. 2002. Singlet oxygen production in herbicide-
724 treated photosystem II. FEBS **532**, 407–410.
725 **Hanaoka H, Noda T, Shirano Y, Kato T, Hayashi H, Shibata D, Tabata S, Ohsumi Y**. 2002. Leaf
726 senescence and starvation-induced chlorosis are accelerated by the disruption of an
727 Arabidopsis autophagy gene. Plant Physiol **129**, 1181–1193.
728 **Heath RL, Packer L**. 1968. Photoperoxidation in isolated chloroplasts. Archives of Biochemistry
729 and Biophysics **125**, 189–198.
730 **Izumi M, Ishida H, Nakamura S, Hidema J**. 2017. Entire photodamaged chloroplasts are
731 transported to the central vacuole by autophagy. Plant Cell **29**, 377–394.
732 **Karpinska B, Wingsle G, Karpinski S**. 2000. Antagonistic effects of hydrogen peroxide and
733 glutathione on acclimation to excess excitation energy in Arabidopsis. IUBMB Life **50**, 21–26.
734 **Karpinski S, Reynolds H, Karpinska B, Wingsle G, Creissen G, Mullineaux P**. 1999. Systemic
735 signaling and acclimation in response to excess excitation energy in Arabidopsis. Science **284**,
736 654–7.
737 **Kim C, Apel K**. 2013. 1O2-mediated and EXECUTER-dependent retrograde plastid-to-nucleus
738 signaling in norflurazon-treated seedlings of arabidopsis thaliana. Molecular Plant **6**, 1580–
739 1591.
740 **Laloi C, Stachowiak M, Pers-Kamczyc E, Warzych E, Murgia I, Apel K**. 2007. Cross-talk between
741 singlet oxygen- and hydrogen peroxide-dependent signaling of stress responses in Arabidopsis
742 thaliana. Proceedings of the National Academy of Sciences of the United States of America
743 **104**, 672–677.
744 **Lascano R, Munoz N, Robert G, Rodriguez M, Melchiorre M, Trippi V, Quero G**. 2012.
745 Paraquat: An Oxidative Stress Inducer. Herbicides - Properties, Synthesis and Control of
746 Weeds. London: IntechOpen, 135–148.
747 **Lemke MD, Fisher KE, Kozlowska MA, Tano DW, Woodson JD**. 2021. The core autophagy
748 machinery is not required for chloroplast singlet oxygen - mediated cell death in the
749 Arabidopsis thaliana plastid ferrochelatase two mutant. BMC plant biology **21**, 1–20.
750 **Liu Y, Xiong Y, Bassham DC**. 2009. Autophagy is required for tolerance of drought and salt
751 stress in plants. Autophagy **5**, 954–63.
752 **Liubimovskii SO, Ustynyuk LY, Tikhonov AN**. 2021. Superoxide radical scavenging by sodium
753 4,5-dihydroxybenzene-1,3-disulfonate dissolved in water: Experimental and quantum chemical
754 studies. Journal of Molecular Liquids **333**, 20–23.
755 **Livak KJ, Schmittgen TD**. 2001. Analysis of relative gene expression data using real-time
756 quantitative PCR and the 2(-Delta Delta CT) Method. Methods **25**, 402–408.
757 **Mallén-ponce MJ, Pérez-pérez ME**. 2023. Redox-mediated activation of ATG3 promotes ATG8
758 lipidation and autophagy progression in Chlamydomonas reinhardtii. Plant physiology **00**, 1–
759 17.
760 **Mansouri A, Makris DP, Kefalas P**. 2005. Determination of hydrogen peroxide scavenging
761 activity of cinnamic and benzoic acids employing a highly sensitive peroxyoxalate
762 chemiluminescence-based assay: Structure-activity relationships. Journal of Pharmaceutical
763 and Biomedical Analysis **39**, 22–26.
764 **Masclaux-Daubresse C, Clement G, Anne P, Routaboul J-M, Guiboileau A, Soulay F, Shirasu K,**
765 **Yoshimoto K**. 2014. Stitching together the Multiple Dimensions of Autophagy Using
766 Metabolomics and Transcriptomics Reveals Impacts on Metabolism, Development, and Plant
767 Responses to the Environment in Arabidopsis. The Plant Cell **26**, 1857–1877.
768 **Mehler AH**. 1951. Studies on reactions of illuminated chloroplasts. II. Stimulation and
769 inhibition of the reaction with molecular oxygen. Archives of Biochemistry and Biophysics **34**,
770 339–351.
771 **Melchiorre M, Robert G, Trippi V, Racca R, Lascano HR**. 2009. Superoxide dismutase and
772 glutathione reductase overexpression in wheat protoplast: photooxidative stress tolerance and

773 changes in cellular redox state. Plant Growth Regulation **57**, 57–68.
774 **Meskauskiene R, Nater M, Goslings D, Kessler F, Op den Camp R, Apel K**. 2001. FLU: A
775 negative regulator of chlorophyll biosynthesis in arabidopsis thaliana. Proceedings of the
776 National Academy of Sciences of the United States of America **98**, 12826–12831.
777 **Munch D, Rodriguez E, Bressendorff S, Park OK, Hofius D, Petersen M**. 2014. Autophagy
778 deficiency leads to accumulation of ubiquitinated proteins, ER stress, and cell death in
779 Arabidopsis. Autophagy **10**, 1579–1587.
780 **Nakamura S, Hagihara S, Otomo K, Ishida H, Hidema J, Nemoto T, Izumi M**. 2021. Autophagy
781 Contributes to the Quality Control of Leaf Mitochondria. Plant & cell physiology **62**, 229–247.
782 **Nakamura S, Hidema J, Sakamoto W, Ishida H, Izumi M**. 2018. Selective Elimination of
783 Membrane-Damaged Chloroplasts via microautophagy. Plant Physiology **177**, 1007–1026.
784 **Navabpour S, Morris K, Allen R, Harrison E, A-H-Mackerness S, Buchanan-Wollaston V**. 2003.
785 Expression of senescence-enhanced genes in response to oxidative stress. Journal of
786 experimental botany **54**, 2285–92.
787 **Nazish T, Huang YJ, Zhang J, Xia JQ, Alfatih A, Luo C, Cai XT, Xi J, Xu P, Xiang C Bin**. 2022.
788 Understanding paraquat resistance mechanisms in Arabidopsis thaliana to facilitate the
789 development of paraquat-resistant crops. Plant Communications **3**, 1–11.
790 **Nietzel T, Elsässer M, Ruberti C, *et al.*** 2019. The fluorescent protein sensor roGFP2-Orp1
791 monitors in vivo H2O2 and thiol redox integration and elucidates intracellular H2O2 dynamics
792 during elicitor-induced oxidative burst in Arabidopsis. New Phytologist **221**, 1649–1664.
793 **Oikawa K, Goto-yamada S, Hayashi Y, *et al.*** 2022. Pexophagy suppresses ROS-induced damage
794 in leaf cells under high-intensity light. Nature Communications **13**.
795 **Op Den Camp RGL, Przybyla D, Ochsenbein C, *et al.*** 2003. Rapid Induction of Distinct Stress
796 Responses after the Release of Singlet Oxygen in Arabidopsis. Plant Cell **15**, 2320–2332.
797 **Peláez-vico MÁ, Fichman Y, Zandalinas SI, Van F, Karpiński SM, Mittler R**. 2022. ROS and
798 redox regulation of cell-to-cell and systemic signaling in plants during stress. Free Radical
799 Biology and Medicine.
800 **Pérez-Pérez ME, Couso I, Crespo JL**. 2012*a*. Carotenoid deficiency triggers autophagy in the
801 model green alga Chlamydomonas reinhardtii. Autophagy **8**, 376–388.
802 **Pérez-Pérez ME, Lemaire SD, Crespo JL**. 2012*b*. Reactive oxygen species and autophagy in
803 plants and algae. Plant physiology **160**, 156–64.
804 **Pérez-Pérez ME, Lemaire SD, Crespo JL**. 2016. Control of Autophagy in *Chlamydomonas* Is
805 Mediated through Redox-Dependent Inactivation of the ATG4 Protease. Plant Physiology **172**,
806 2219–2234.
807 **Pérez-Pérez ME, Zaffagnini M, Marchand CH, Crespo JL, Lemaire SD**. 2014. The yeast
808 autophagy protease Atg4 is regulated by thioredoxin. Autophagy **10**, 1–12.
809 **Qi H, Xia FN, Xiao S**. 2021. Autophagy in plants: Physiological roles and post-translational
810 regulation. Journal of Integrative Plant Biology **63**, 161–179.
811 **Di Rienzo JA, Guzmán AW, Casanoves F**. 2002. A multiple-comparisons method based on the
812 distribution of the root node distance of a binary tree. Journal of Agricultural, Biological, and
813 Environmental Statistics **7**, 129–142.
814 **Robert G, Melchiorre M, Racca R, Trippi V, Lascano HR**. 2009. Apoplastic superoxide level in
815 wheat protoplast under photooxidative stress is regulated by chloroplast redox signals : Effects
816 on the antioxidant system. Plant Science **177**, 168–174.
817 **Robert G, Muñoz N, Alvarado-Affantranger X, Saavedra L, Davidenco V, Rodríguez-Kessler M,**
818 **Estrada-Navarrete G, Sánchez F, Lascano R**. 2018. Phosphatidylinositol 3-kinase function at
819 very early symbiont perception: A local nodulation control under stress conditions? Journal of
820 Experimental Botany **69**, 2037–2048.
821 **Robert G, Muñoz N, Melchiorre M, Sánchez F, Lascano R**. 2014. Expression of animal anti-
822 apoptotic gene Ced-9 enhances tolerance during Glycine max L.-Bradyrhizobium japonicum
823 interaction under saline stress but reduces nodule formation. PLoS One **9**, e101747.
824 **Robert G, Yagyu M, Koizumi T, Naya L, Masclaux-Daubresse C, Yoshimoto K**. 2021.

Ammonium stress increases microautophagic activity while impairing macroautophagic flux in Arabidopsis roots. Plant Journal **105**, 1083–1097.

Rubin G, Tohge T, Matsuda F, Saito K, Scheible W-R. 2009. Members of the LBD Family of Transcription Factors Repress Anthocyanin Synthesis and Affect Additional Nitrogen Responses in Arabidopsis. The Plant Cell **21**, 3567–3584.

Sabater B, Martín M. 2013. Hypothesis: Increase of the ratio singlet oxygen plus superoxide radical to hydrogen peroxide changes stress defense response to programmed leaf death. Frontiers in Plant Science **4**, 1–8.

Scarpeci TE, Zanor MI, Carrillo N, Mueller-Roeber B, Valle EM. 2008. Generation of superoxide anion in chloroplasts of Arabidopsis thaliana during active photosynthesis : a focus on rapidly induced genes. Plant Mol Biol **66**, 361–378.

Scharfenberg M, Mittermayr L, Von Roepenack-Lahaye E, Schlicke H, Grimm B, Leister D, Kleine T. 2015. Functional characterization of the two ferrochelatases in Arabidopsis thaliana. Plant Cell and Environment **38**, 280–298.

Schwarzla M, Dick TP, Meyer AJ, Morgan B. 2015. Dissecting Redox Biology Using Fluorescent Protein Sensors 1. **00**.

Schwarzländer M, Dick TP, Meyer AJ, Morgan B. 2015. Dissecting redox biology using fluorescent protein sensors. Antioxidants and Redox Signaling **24**, 680–712.

Schwarzlander M, Fricker MD, Muller C, Marty L, Brach T, Novak J, Sweetlove LJ, Hell R, Meyer AJ. 2008. Confocal imaging of glutathione redox potential in living plant cells. Journal of Microscopy **231**, 299–316.

Schwarzländer M, Fricker MD, Sweetlove LJ. 2009. Monitoring the in vivo redox state of plant mitochondria: effect of respiratory inhibitors, abiotic stress and assessment of recovery from oxidative challenge. Biochimica et biophysica acta **1787**, 468–75.

Shao N, Duan GY, Bock R, Molekulare M. 2013. A Mediator of Singlet Oxygen Responses in Chlamydomonas reinhardtii and Arabidopsis Identi fi ed by a Luciferase-Based Genetic Screen in Algal Cells. The Plant Cell **25**, 4209–4226.

Shao N, Krieger-liszkay A, Schroda M, Beck CF. 2007. A reporter system for the individual detection of hydrogen peroxide and singlet oxygen : its use for the assay of reactive oxygen species produced in vivo. The Plant journal **50**, 475–487.

Shibata M, Oikawa K, Yoshimoto K, Kondo M, Mano S, Yamada K, Hayashi M, Sakamoto W, Ohsumi Y, Nishimura M. 2013. Highly Oxidized Peroxisomes Are Selectively Degraded via Autophagy in Arabidopsis. The Plant cell **25**, 4967–83.

Signorelli S, Tarkowski ŁP, Van den Ende W, Bassham DC. 2019. Linking Autophagy to Abiotic and Biotic Stress Responses. Trends in Plant Science **24**, 413–430.

Su T, Li X, Yang M, Shao Q, Zhao Y, Ma C, Wang P. 2020. Autophagy: An Intracellular Degradation Pathway Regulating Plant Survival and Stress Response. Frontiers in Plant Science **11**, 1–16.

Triantaphylidès C, Krischke M, Hoeberichts FA, Ksas B, Gresser G, Havaux M, Van Breusegem F, Mueller MJ. 2008. Singlet oxygen is the major reactive oxygen species involved in photooxidative damage to plants. Plant Physiology **148**, 960–968.

Trippi VS, Lascano HR, Melchiorre M. 2009. Plant senescence: A self-induced process. Current topics in plant biology **10**, 1–15.

Velika B, Kron I. 2012. Antioxidant properties of benzoic acid derivatives against Superoxide radical. Free Radicals and Antioxidants **2**, 62–67.

Wang P, Wang T, Han J, Li M, Zhao Y, Su T, Ma C. 2021. Plant Autophagy : An Intricate Process Controlled by Various Signaling Pathways. Frontiers in Plant Science **12**, 754982.

Willems P, Mhamdi A, Stael S, Storme V, Kerchev P, Noctor G, Gevaert K, Van Breusegem F. 2016. The ROS wheel: Refining ROS transcriptional footprints. Plant Physiology **171**, 1720–1733.

Wintermans M. j. FG, De Mots A. 1965. SPECTROPHOTOMETRIC CHARACTERISTICS OF CHLOROPHYLLS a AND b AND THEIR PHEOPHYTINS IN ETHANOL. Biochimica et biophysica acta

877 **109**, 448–453.
878 **Woodson JD**. 2019. Chloroplast stress signals: regulation of cellular degradation and
879 chloroplast turnover. Current Opinion in Plant Biology **52**, 30–37.
880 **Xiong Y, Contento AL, Bassham DC**. 2007*a*. Disruption of Autophagy Results in Constitutive
881 Oxidative Stress in Arabidopsis. Autophagy **3**, 257–258.
882 **Xiong Y, Contento AL, Nguyen PQ, Bassham DC**. 2007*b*. Degradation of oxidized proteins by
883 autophagy during oxidative stress in Arabidopsis. Plant physiology **143**, 291–9.
884 **Yagyu M, Yoshimoto K**. 2023. New Insights into Plant Autophagy: Molecular Mechanisms and
885 Roles in Development and Stress Responses. Journal of experimental botany, 1–28.
886 **Yang M, Bu F, Huang W, Chen L**. 2019. Multiple regulatory levels shape autophagy activity in
887 plants. Frontiers in Plant Science **10**, 1–7.
888 **Yoshimoto K, Hanaoka H, Sato S, Kato T, Tabata S, Noda T, Ohsumi Y**. 2004. Processing of
889 ATG8s , Ubiquitin-Like Proteins , and Their Deconjugation by ATG4s Are Essential for Plant
890 Autophagy. The Plant Cell **16**, 2967–2983.
891 **Yoshimoto K, Jikumaru Y, Kamiya Y, Kusano M, Consonni C, Panstruga R, Ohsumi Y, Shirasu**
892 **K**. 2009. Autophagy negatively regulates cell death by controlling NPR1-dependent salicylic
893 acid signaling during senescence and the innate immune response in Arabidopsis. The Plant
894 cell **21**, 2914–27.
895 **Zheng X, Yang Z, Gu Q, Xia F, Fu Y, Liu P, Yin XM, Li M**. 2020. The protease activity of human
896 ATG4B is regulated by reversible oxidative modification. Autophagy **16**, 1838–1850.
897 **Zhou J, Wang J, Cheng Y, Chi YJ, Fan B, Yu JQ, Chen Z**. 2013. NBR1-Mediated Selective
898 Autophagy Targets Insoluble Ubiquitinated Protein Aggregates in Plant Stress Responses. PLoS
899 Genetics **9**.
900 **Zhuang X, Cui Y, Gao C, Jiang L**. 2015. Endocytic and autophagic pathways crosstalk in plants.
901 Current Opinion in Plant Biology **28**, 39–47.
902
903 **Figure legends**

904 **Figure 1:** Autophagic flux and cytoplasmic redox state in *Arabidopsis thaliana* plants exposed to
905 different abiotic stress conditions. (A-C) Seven-day old 35S:GFP-ATG8a transgenic plants and
906 cytosol-targeted fluorescent redox sensors GFP2-Orp1 and GRX-roGFP2 expressing plants were
907 exposed to different stress conditions in MS liquid medium. To induce autophagic bodies
908 accumulation, MS liquid medium was supplemented with 1 µM Concanamycin A. (A)
909 Representative images showing autophagic bodies accumulation and cytoplasmic redox state.
910 The stress treatments were performed for 16 h, followed by the evaluation of autophagic bodies
911 accumulation (GFP-ATG8 columns) and the cytoplasmic redox state (GRX-roGFP and GFP2-Orp1
912 columns) by confocal microscopy. Arrowheads indicate some of the autophagic bodies
913 observed. Scale bars: 30 µm. GRX-roGFP and GFP2-Orp1 columns are ratiometric images. For
914 pseudocolor display, the ratio was coded on a spectral color scale ranging from blue (fully
915 reduced) to red (fully oxidized). The treatments included: MS with nitrogen (control), MS with
916 nitrogen in darkness (-C), MS without nitrogen (-N), MS with nitrogen supplemented with 100
917 mM mannitol (Manitol), 50 mM NaCl (NaCl), 1 µM methyl viologen (MV) and 10 mM H_2O_2. (B)
918 Quantification of autophagic body accumulation was performed using single-plane confocal
919 images. Two sections from at least 6 plants were analyzed. (C) Quantification of cytoplasmic
920 redox state expressed as the ratio of the fluorescence intensities measured at 488 nm and 405
921 nm. At least 4 plants were analyzed. Statistically significant differences are indicated by asterisks
922 (*$P < 0.05$; error bars: means ± SEM, DGC test).
923
924 **Figure 2:** Treatments with MV and H_2O_2 highly oxidized the cytoplasm and prevented autophagy
925 induction in Arabidopsis. (A-C) Seven-day old 35S:GFP-ATG8a transgenic plants and cytosol-
926 targeted fluorescent redox sensors GFP2-Orp1 and GRX-roGFP2 expressing plants were exposed
927 to autophagy-inducing conditions and the effect of methyl viologen (MV) and H_2O_2 on

928 autophagic flux and cytoplasmic redox state were analyzed. (A) Representative images showing
929 autophagic bodies accumulation and cytoplasmic redox state. The stress treatments were
930 performed for 16 h, followed by the evaluation of autophagic bodies accumulation (GFP-ATG8
931 columns) and the cytoplasmic redox state (GRX-roGFP and GFP2-Orp1 columns) by confocal
932 microscopy. To induced autophagic bodies accumulation, MS liquid medium was supplemented
933 with 1 µM Concanamycin A. Arrowheads indicate some of the autophagic bodies observed. Scale
934 bars: 30 µm. GRX-roGFP and GFP2-Orp1 columns are ratiometric images. The treatments
935 included: MS with nitrogen (control), MS with nitrogen in darkness (-C) supplemented with 10
936 mM H_2O_2 (-C + H_2O_2), MS without nitrogen (-N) supplemented with 1 µM methyl viologen (-N +
937 MV) or 10 mM H_2O_2 (-N + H_2O_2). 10 mM Tiron and 10 mM Benzoic acid (BA) were used for ROS
938 scavenging (-N + MV + Tiron and -N + MV + BA). (B) Quantification of autophagic body
939 accumulation was performed using single-plane confocal images. Two sections from at least 6
940 plants were analyzed. Two sections from at least 6 plants were analyzed. (C) Quantification of
941 cytoplasmic redox state expressed as the ratio of the fluorescence intensities measured at 488
942 nm and 405 nm. At least 4 plants were analyzed. (D) Effects of oxidative treatments on the
943 autophagic flux evaluated through the degradation of the GFP-ATG8a fusion protein by western
944 blot. Seven-day old 35S:GFP-ATG8a transgenic Arabidopsis seedlings were exposed to the
945 different treatments for 6-8 h. The GFP-ATG8a fusion has a predicted molecular weight of
946 approximately 40 kDa (closed arrowheads); free GFP has a predicted molecular weight of 27 kDa
947 (open arrowheads). Representative images are shown. Ratio: the numbers in brackets denote
948 the GFP/GFP-ATG8 ratio normalized to the control condition (well 1 in each box). Three
949 replicates were performed (more than fifteen plants per replicate). HL: high light treatment
950 (≈1000 µmoles m^{-2} s^{-1}). Asterisks indicate statistically significant differences (*P < 0.05; error
951 bars: means ± SEM, DGC test).
952
953
954 **Figure 3:** Autophagy is induced after oxidative stress treatments in Arabidopsis. (A-D) Seven-day
955 old transgenic plants expressing 35S:GFP-ATG8a and cytosol-targeted fluorescent redox sensors
956 GFP2-Orp1 and GRX-roGFP2 were subjected to a brief exposure of oxidative stress, either 10
957 mM H_2O_2 or high light intensity (≈1000 µmoles m^{-2} s^{-1}), for 4 h. Subsequently they were
958 transferred to MS liquid medium for a 20-hour recovery period under continuous light (≈120
959 µmoles m^{-2} s^{-1}) (recovery). Control plants were incubated under continuous light (≈120 µmoles
960 m^{-2} s^{-1}) in H_2O_2-free MS liquid medium for 24 h. Stressed plants were incubated in MS
961 supplemented with 10 mM H_2O_2 or high light intensity (≈1000 µmoles m^{-2} s^{-1}) for 24 h. (A)
962 Representative images showing autophagic bodies accumulation and cytoplasmic redox state.
963 To induce accumulation of autophagic bodies, MS liquid medium was supplemented with 1 µM
964 Concanamycin A. Arrowheads indicate some of the autophagic bodies observed. Scale bars: 30
965 µm. GRX-roGFP and GFP2-Orp1 columns represent ratiometric images, with pseudocolor display
966 indicating the ratio on a spectral color scale ranging from blue (fully reduced) to red (fully
967 oxidized). (B) Quantification of autophagic body accumulation was performed using single-plane
968 confocal images. Two sections from at least 6 plants were analyzed. (C) Quantification of
969 cytoplasmic redox state expressed as the ratio of the fluorescence intensities measured at 488
970 nm and 405 nm. At least 4 plants were analyzed. Asterisks indicate statistically significant
971 differences (*P < 0.05; error bars: means ± SEM, DGC test). (D) Autophagic flux evaluated
972 through the degradation of the GFP-ATG8a fusion protein by western blot. Total protein (40 µg)
973 was subjected to immunoblot analysis with anti-GFP antibodies. The GFP-ATG8a fusion has a
974 predicted molecular weight of approximately 40 kDa (closed arrowheads), while free GFP has a
975 predicted molecular weight of 27 kDa (open arrowheads). Representative images are shown.
976 The numbers in brackets denote the GFP/GFP-ATG8 ratio normalized to the control condition.
977 Three replicates were performed (more than fifteen plants per replicate). Asterisks indicate
978 statistically significant differences (*P < 0.05; error bars: means ± SEM, DGC test).
979

980

981 **Figure 4:** DCMU and methylene blue treatments induced autophagic flux in Arabidopsis. (A-D)
982 Seven-day old transgenic plants expressing 35S:GFP-ATG8a and cytosol-targeted fluorescent
983 redox sensors GFP2-Orp1 and GRX-roGFP2 were incubated in MS medium supplemented with
984 either 20 µM 3-(3,4-dichlorophenyl)-1,1-dimethylurea (DCMU) or 20 µM methylene blue (MB),
985 and the autophagic flux and cytoplasmic redox state were evaluated. (A) Representative images
986 showing autophagic bodies accumulation and cytoplasmic redox state after 16 h of treatment.
987 To induce autophagic bodies accumulation, MS liquid medium was supplemented with 1 µM
988 Concanamycin A. Some of the autophagic bodies are indicated by arrowheads. Scale bars: 30
989 µm. The GRX-roGFP and GFP2-Orp1 columns represent ratiometric images. For pseudo color
990 display, the ratio was coded using a spectral color scale ranging from blue (fully reduced) to red
991 (fully oxidized). (B) Quantification of autophagic body accumulation was performed using single-
992 plane confocal images. Two sections from at least 6 plants were analyzed. (C) Quantification of
993 cytoplasmic redox state expressed as the ratio of the fluorescence intensities measured at 488
994 nm and 405 nm. Analysis was performed on at least 4 plants. Asterisks indicate statistically
995 significant differences (*P < 0.05; error bars: means ± SEM, DGC test). (D) Evaluation of the
996 effects of DCMU and MB on autophagic flux through degradation of the GFP-ATG8a fusion
997 protein by western blot. Seven-day old transgenic Arabidopsis seedlings expressing 35S:GFP-
998 ATG8a were exposed to the different treatments for 6-8 h. Total protein (40 µg) was subjected
999 to immunoblot analysis with anti-GFP antibodies. The GFP-ATG8a fusion has a predicted
1000 molecular weight of approximately 40 kDa (closed arrowheads), while free GFP has a predicted
1001 molecular weight of 27 kDa (open arrowheads). Representative images are shown. The numbers
1002 in brackets denote the GFP/GFP-ATG8 ratio normalized to control condition. Four replicates
1003 were performed with more than fifteen plants per replicate. (E) Seven-day old Arabidopsis
1004 seedlings were exposed to the different treatments and soluble sugar content was analyzed.
1005 FW: fresh weight. Asterisks indicate statistically significant differences (*P < 0.05; error bars:
1006 means ± SEM, DGC test).

1007

1008 **Figure 5:** Autophagic flux is induced in conditionally chloroplast $^1O_2$-hyperproducing *flu* mutant
1009 Arabidopsis plants. (A-C) Seven-day old wildtype (Col-0) and *flu* mutant plants expressing
1010 35S:GFP-ATG8a or GFP2-Orp1 were transferred to darkness for 8 h, followed by re-exposure to
1011 light. Control plants were maintained under continuous light conditions. After 8 h, the
1012 autophagic flux and cytoplasmic redox state were analyzed. (A) Representative images showing
1013 autophagic bodies accumulation and cytoplasmic redox state. To induce autophagic bodies
1014 accumulation, the MS liquid medium was supplemented with 1 µM Concanamycin A. The GFP2-
1015 Orp1 columns represent ratiometric images. For pseudocolor display, the ratio was coded on a
1016 spectral color scale ranging from blue (fully reduced) to red (fully oxidized). Arrowheads indicate
1017 some of the autophagic bodies observed. Scale bars: 30 µm. (B) Quantification of autophagic
1018 body accumulation was performed using single-plane confocal images. Two sections from at
1019 least 6 plants were analyzed. (C) Quantification of cytoplasmic redox state expressed as the ratio
1020 of the fluorescence intensities measured at 488 nm and 405 nm. At least 4 plants were analyzed.
1021 Asterisks indicate statistically significant differences (*P < 0.05; error bars: means ± SEM, DGC
1022 test). (D) Evaluation of autophagic flux through the degradation of the GFP-ATG8a fusion protein
1023 by western blot. Seven-day old wildtype (Col-0) and *flu* mutant plants expressing 35S:GFP-ATG8a
1024 were transferred to darkness for 8 h and then re-exposed to light for 6 h (after darkness).
1025 Continuous light was used as a control (light). Total protein (40 µg) was subjected to immunoblot
1026 analysis with anti-GFP antibodies. The GFP-ATG8a fusion has a predicted molecular weight of
1027 approximately 40 kDa (closed arrowheads); while free GFP has a predicted molecular weight of

27 kDa (open arrowheads). Representative images are shown. The numbers in brackets denote the GFP/GFP-ATG8 ratio normalized to *flu* mutans under control condition. Three replicates were performed (more than fifteen plants per replicate). Asterisks indicate statistically significant differences.

FIGURE 1

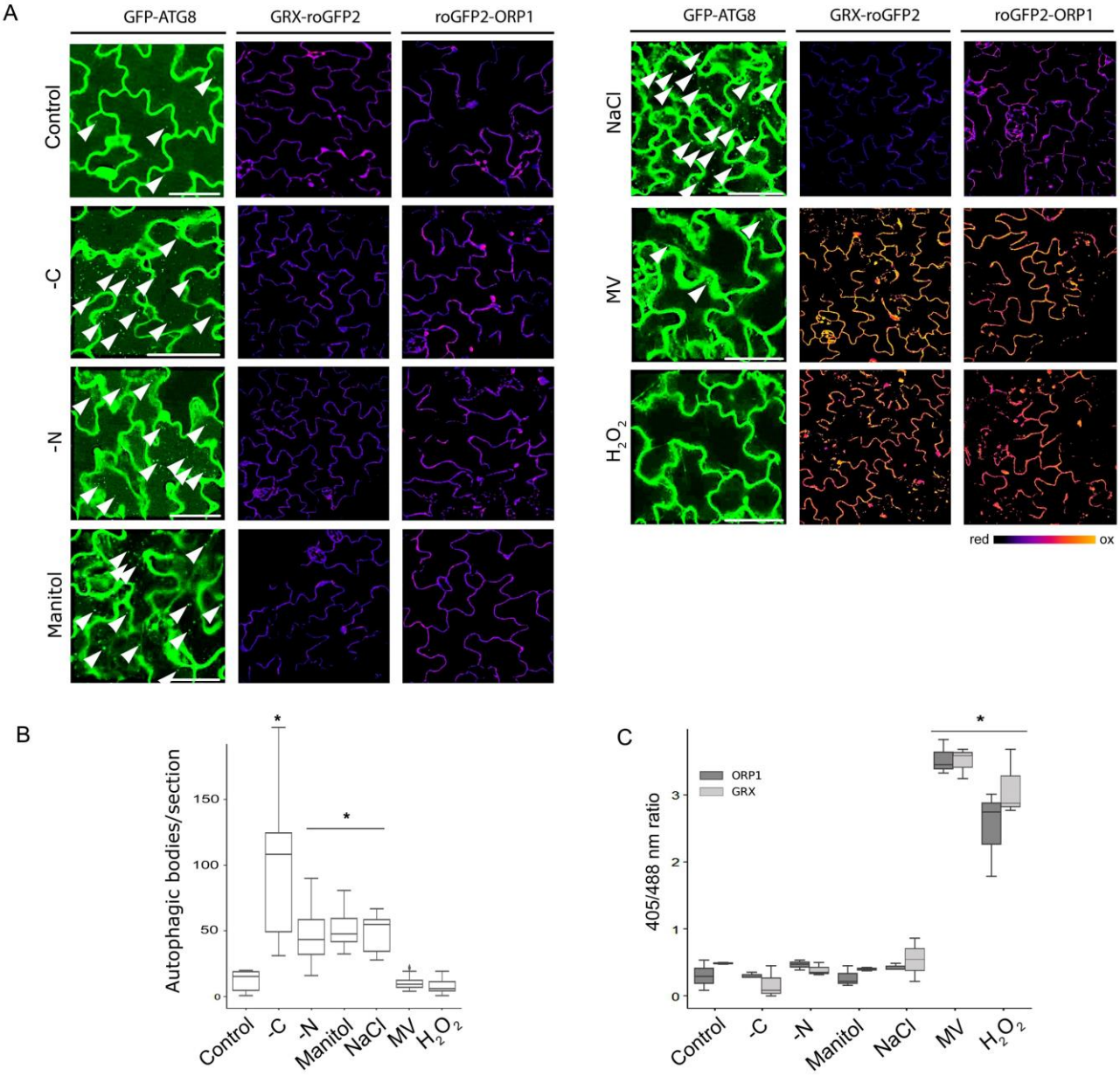

1037 **FIGURE 2**

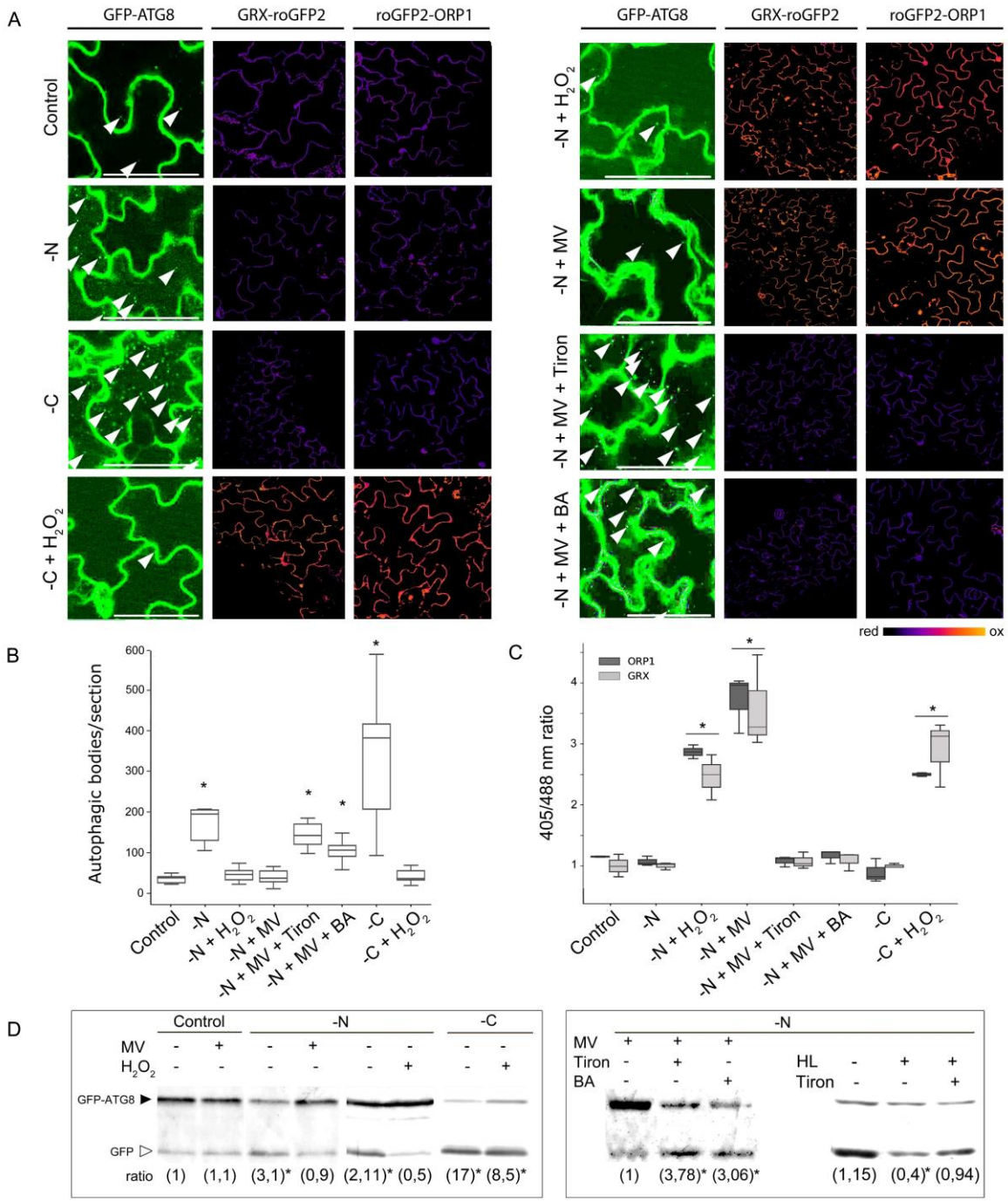

1038

1039

1040

1041

1042

1043

1044 **FIGURE 3**

1045

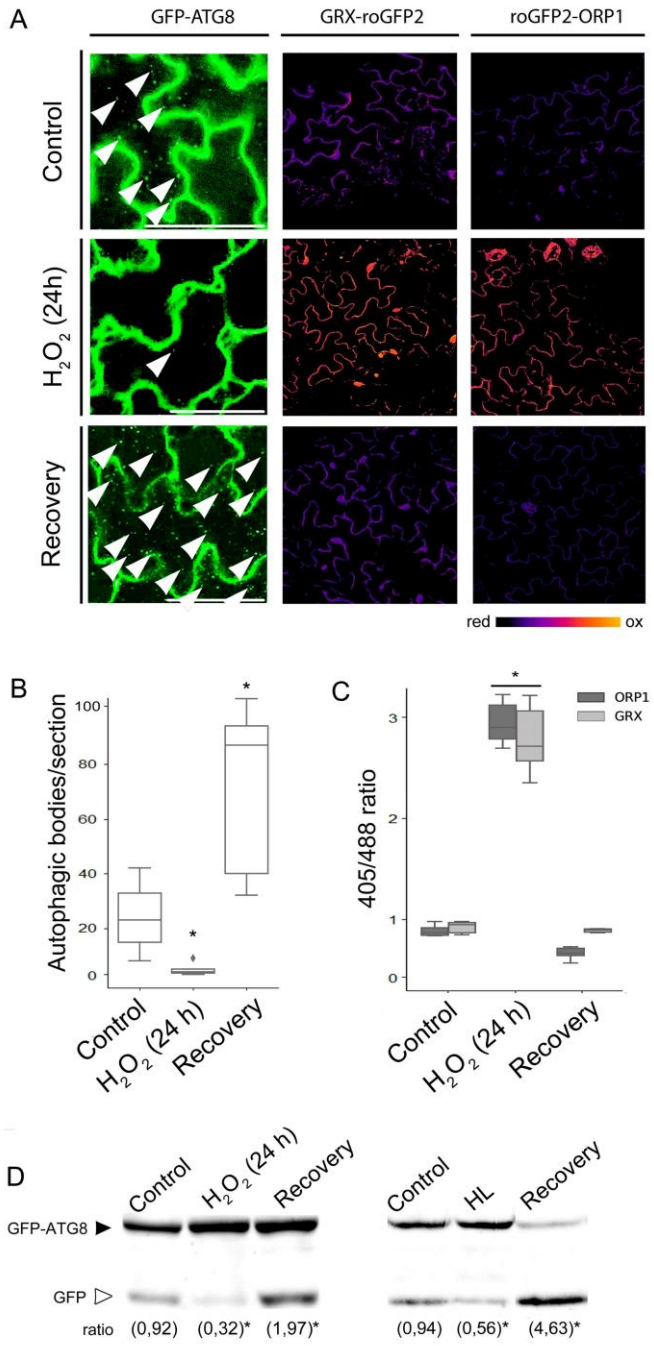

1046
1047
1048
1049
1050
1051
1052
1053

1054 **FIGURE 4**

1055

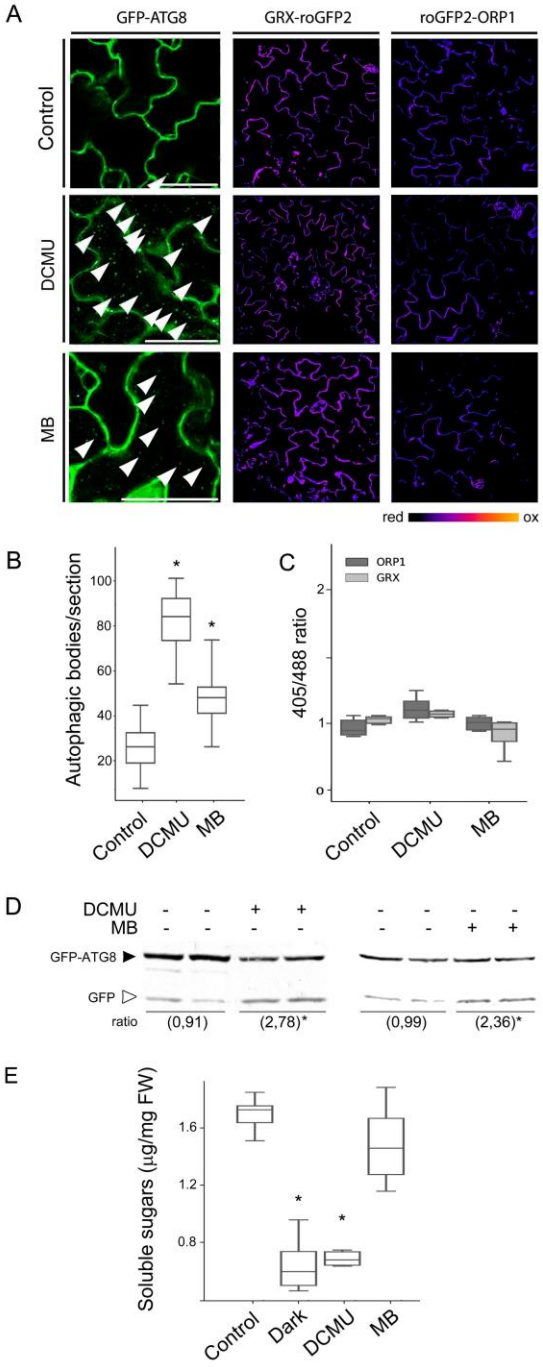

1056

1057

1058

1059

1060

1061

1062 **FIGURE 5**

1063

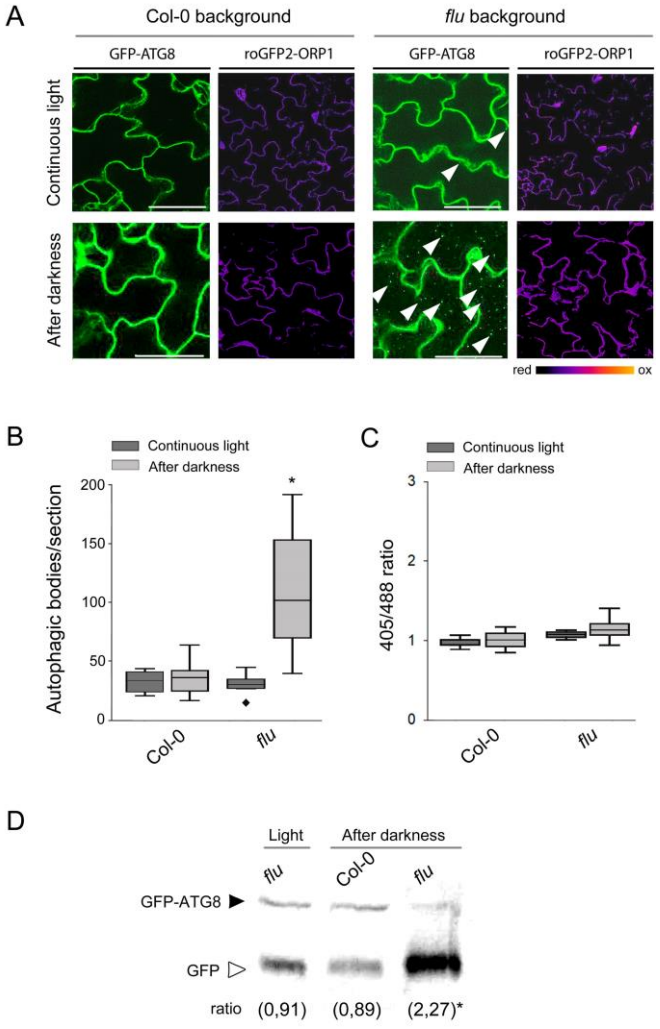

1064

1065

1066

1067